

Influence of oxygen on electronic correlation and transport in iron in the outer Earth's core

G. G. Blesio,¹ L. V. Pourovskii,^{2,3} M. Aichhorn,⁴ M. Pozzo,⁵ D. Alfè,^{5,6} and J. Mravlje¹

¹*Jožef Stefan Institute, Jamova 39, SI-1000 Ljubljana, Slovenia**

²*CPHT, CNRS, Ecole polytechnique, Institut Polytechnique de Paris, Route de Saclay, 91128 Palaiseau, France.*

³*Collège de France, 11 place Marcelin Berthelot, 75005 Paris, France.*

⁴*Institute of Theoretical and Computational Physics, Graz University of Technology, NAWI Graz, Petersgasse 16, Graz, 8010, Austria*

⁵*Department of Earth Sciences and London Centre for Nanotechnology, University College London, Gower Street, London WC1E 6BT, UK*

⁶*Dipartimento di Fisica Ettore Pancini, Università di Napoli Federico II, Monte S. Angelo, I-80126 Napoli, Italy.*

Knowing the transport properties of iron under realistic conditions present in the Earth's core is essential for the geophysical modeling of Earth's magnetic field generation. Besides by extreme pressures and temperatures, transport may be influenced importantly also by the presence of light elements. Using a combination of molecular dynamics, density functional theory, and dynamical mean-field theory methods we investigate how oxygen impurities influence the electronic correlations and transport in the liquid outer Earth's core. We consider a case with an oxygen content of ~ 10 atomic%, a value that is believed to be close to the composition of the core. We find that the electronic correlations are enhanced but their effect on conductivities is moderate (compared to pure Fe, electrical conductivity drops by 10% and thermal conductivity by 18%). The effect of electron-electron scattering alone, whereas not large, is comparable to effects of the compositional disorder. We reveal the mechanism behind the larger suppression of the thermal conductivity and associated reduction of the Lorenz ratio and discuss its geophysical significance.

INTRODUCTION

The Earth's magnetic field is generated by a self-excited dynamo that is driven by convection in the outer core. The thermal conductivity of iron, which determines the amount of heat flow available for convection, and the value of electrical conductivity, which determines the dissipation of the current, are crucial inputs for geophysical models of this geodynamo mechanism. Direct measurements of transport under extreme pressures and temperatures that are relevant to Earth's core are challenging [1, 2] as one must ensure homogeneous temperature and carefully control the geometry of the samples [3].

One can access transport properties also from first principle calculations based on the molecular dynamics (MD)–density functional theory (DFT) method [4–6]. These calculations have shown that the electrical and thermal conductivities have values that are significantly (2–3 times) higher [5, 6] than earlier established estimates [7, 8]. These earlier estimates were based on extrapolations that neglected the effects of resistivity saturation [9–11]. The higher values of thermal conductivity lead to a different geophysical picture, with an inner core that is younger (< 1 billion years, whereas magnetism is known to exist for at least 3.4 billion years [12, 13]), and less thermal convective energy to drive the geodynamo, which is known as “the new core paradox” [14]. Namely, less thermal energy implies that convection must be helped by the chemical convection driven by the exso-

lution of lighter elements but this was less active before the formation of the inner core.

There has been an ongoing discussion on whether electronic correlations, which have been shown to be significant in iron under Earth's core conditions [15, 16], can cause a breakdown in the Mott-Ioffe-Regel resistivity saturation [9, 17]. This debate revolves around whether these correlations are strong enough to reduce conductivity values to previously established levels [18–20], as suggested in a pioneering work (later retracted)[18]. Recent findings indicate that electron-electron scattering (EES) plays only a moderate role and represents a small fraction compared to thermal-disorder (electron-phonon) scattering [21, 22].

One important question remains to be addressed: does alloying with lighter elements significantly enhance correlations, and if so, to what extent are conductivities suppressed? The Earth's core contains a sizable contribution of lighter elements, primarily silicon and oxygen, with recent research indicating a high oxygen concentration [23]. The influence of these substitutions has been broadly investigated using MD-DFT [5, 6, 24, 25], but without accounting for correlation effects. Oxygen might enhance electronic correlations by reducing iron 3d shell occupancy toward half-filling [26]. Indeed, recent theoretical work [27] investigated several ordered FeO structures and found a very strong enhancement of electron-electron scattering (EES). However, the impact of thermal disorder on EES was neglected in that study, and the final effect on thermal conductivity, taking into account both EES and electron-phonon scattering, was not evaluated. Furthermore, the impact of EES on conductivity in liquid iron, which is most relevant for the dynamo

* german.blesio@ijs.si

mechanism, was not clarified.

In this study, we investigate the transport properties of Fe and FeO alloys in their liquid state at the inner-core boundary (ICB) and core-mantle boundary (CMB) conditions. We describe the liquid state using MD-DFT and account for electron-electron scattering (EES) using dynamical mean-field theory (DMFT) [20, 21, 28, 29]. Specifically, we focus on the $\text{Fe}_{0.91}\text{O}_{0.09}$ composition and observe that its EES rate increases by $\sim 25\%$ compared to pure iron (Fe), but the conductivities are affected to a lesser extent with only an $\approx 10\%$ drop in electrical conductivity σ and an $\approx 18\%$ drop in thermal conductivity κ . This change is mainly due to band-structure effects rather than a direct increase in EES.

In order to quantify the effects of electronic-correlation on transport we compare the calculated DMFT conductivities with those from the MD-DFT. We find that the inclusion of EES leads to only a moderate reduction of electrical and thermal conductivities by roughly 10% and 20%, respectively. This finding is crucial considering a large body of existing theoretical work that neglects EES [5, 6, 11, 24]. A related study of Fe-Si alloys has shown similar behavior [22]. We discuss why the thermal conductivities are suppressed more than the electrical ones and highlight the geophysical implications of our results.

METHODS

We performed the molecular dynamics calculations using the VASP code [30], using the projected augmented wave method [31, 32] to describe the interactions between the electrons and the ions and expanded the single-particle orbitals as linear combinations of plane waves (PW), including PW with maximum energies of 400 eV. The molecular dynamics simulations were performed by sampling the Brillouin zone using the Γ point only, and a time step was 1 fs. The temperature was controlled using the Nosé [33] thermostat. To compute the DFT electrical and thermal conductivity we used the modified version of VASP by Dejarlais [34].

The DFT+DMFT self-consistent calculations were performed with a local density approximation (LDA) approach in the Wien2K code [35, 36], using the TRIQS library [37–40] for the DMFT and transport calculations. We used a local density-density interaction vertex with interaction parameters $U = 5.0$ eV, $J_H = 0.93$ eV, in agreement with the previous studies on pure iron [19, 21], and solved the impurity problem using the continuous-time hybridization-expansion segment solver [41, 42]. Each calculation was first converged by 25 fully self-consistent DFT+DMFT iterations, where each Monte Carlo run employed 2×10^{10} Monte Carlo moves and 200 moves/measurement. Using the converged Kohn–Sham Hamiltonian, 10 additional DMFT cycles were performed with the number of Monte Carlo moves increased to 10^{11} . To obtain clean data for analytical continuation

that we performed using Maximum Entropy method, 20 additional runs (with 2×10^{11} moves per run) were carried out starting from the same converged value of the DMFT bath Green’s function and resetting the random sequence.

We calculated the conductivities within the Kubo linear-response neglecting the vertex corrections. The electrical and thermal conductivity read [40, 43]

$$\sigma_{\alpha\alpha'} = \frac{e^2}{k_B T} K_{\alpha\alpha'}^0, \quad \kappa_{\alpha\alpha'} = k_B \left[K_{\alpha\alpha'}^2 - \frac{(K_{\alpha\alpha'}^1)^2}{K_{\alpha\alpha'}^0} \right], \quad (1)$$

where α is the direction (x, y or z) and k_B the Boltzmann constant. The kinetic coefficients $K_{\alpha\alpha'}^n$ are

$$K_{\alpha\alpha'}^n = 2\pi\hbar \int d\omega (\beta\omega)^n f(\omega) f(-\omega) \Gamma^{\alpha\alpha'}(\omega, \omega), \quad (2)$$

where 2 is the spin factor, $f(\omega)$ is the Fermi function, and the $\Gamma^{\alpha\alpha'}$ is given by

$$\Gamma^{\alpha\alpha'}(\omega, \omega') = \frac{1}{V} \sum_{\mathbf{k}} \text{Tr} \left(v_{\mathbf{k}}^{\alpha} A_{\mathbf{k}}(\omega) v_{\mathbf{k}}^{\alpha'} A_{\mathbf{k}}(\omega') \right) \quad (3)$$

where V is the unit-cell volume, $A_{\mathbf{k}}(\omega)$ is the DMFT spectral function at momentum \mathbf{k} , and $v_{\mathbf{k}}^{\alpha}$ is the corresponding band velocity in the direction α . We also define the transport distribution

$$\Gamma(\omega) = \sum_{\alpha} \Gamma^{\alpha\alpha}(\omega, \omega). \quad (4)$$

We also calculated the response at finite frequency Ω which yields the optical electrical and thermal conductivity. These are evaluated by Eq.1 using the kinetic coefficients evaluated at a finite frequency Ω

$$K_{\alpha\alpha'}^n(\Omega) = 2\pi\hbar \int d\omega \Gamma^{\alpha\alpha'}(\omega + \Omega/2, \omega - \Omega/2) (\omega + \Omega/2)^n \beta^{n-1} \frac{f(\omega - \Omega/2) - f(\omega + \Omega/2)}{\Omega}. \quad (5)$$

In the momentum sums we retained 14 momentum points. The electron-phonon-only values were calculated using the Kubo-Greenwood approximation as implemented in VASP [34] using 10 momentum points. We checked that upon increasing the number of momentum points further the results vary by less than 1%.

RESULTS

We calculate the liquid phase for 67 atoms: all iron (Fe) or with oxygen ($\text{Fe}_{0.91}\text{O}_{0.09}$). We study the liquid at CMB conditions for a temperature $T = 4400$ K, volume $8.64 \text{ \AA}^3/\text{atom}$ (which corresponds to pressure 132 GPa), and ICB conditions $T = 6350$ K with volume $7.16 \text{ \AA}^3/\text{atom}$ (pressure 330 GPa).

The calculations were performed for three snapshots separated by 5 ps time each and the calculations of transport properties was performed by averaging over the snapshots and spatial directions.

Electronic correlations. Figure 1 displays the imaginary part of self-energies for a single snapshot in the energy range of $[-1, 1]$ eV. Each curve represents a different site/orbital/spin index, and the thick lines indicate an average over all of them. Since the electron-electron scattering rate is $1/\tau = -2\text{Im}\Sigma(\omega \rightarrow 0)$, more negative values of $\text{Im}\Sigma$ indicate stronger electronic correlations. Our results show that the scattering increases significantly in the oxygen-rich case for both ICB and CMB. The distribution of the curves reveals that not only the Fe sites closest to oxygen are affected, but also the spread of the data is wider in the oxygen-rich case, and even the self-energies with the smallest magnitudes are enhanced by oxygen. Overall, the average EES, as given by the average $\text{Im}\Sigma$, increases by 25%.

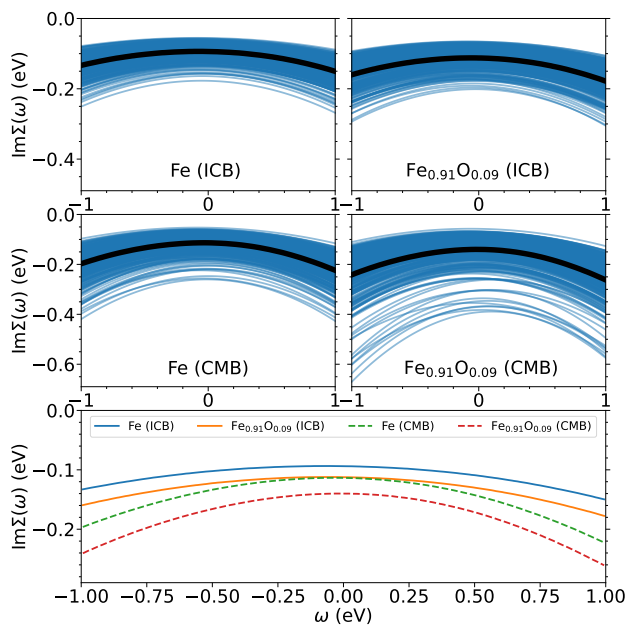


FIG. 1. Imaginary part of the calculated self-energies on the real axis. In the top and middle panels, we show the individual self-energies (blue lines) and their average ($\text{Im}\Sigma$) (black thick). In the bottom panel, the four average self-energies are shown, at the ICB (full) and CMB (dashed) conditions.

Conductivities. The calculated optical conductivities are shown in Fig. 2 for the case of electrical and thermal current on the top and bottom panels, respectively. The $\omega \rightarrow 0$ values indicate the dc-transport values. One sees that quantitatively the effect of oxygen on transport is somewhat weaker than on the EES. Also shown in that figure are the results of a simplified calculation where one uses the $\langle \Sigma \rangle$ instead of the individual self-energies. One sees a “self-averaging” effect: the re-

sults of such a calculation are almost indistinguishable from the full calculation. This also tells that statistical uncertainties of the individual self-energies will not affect the calculated conductivities.

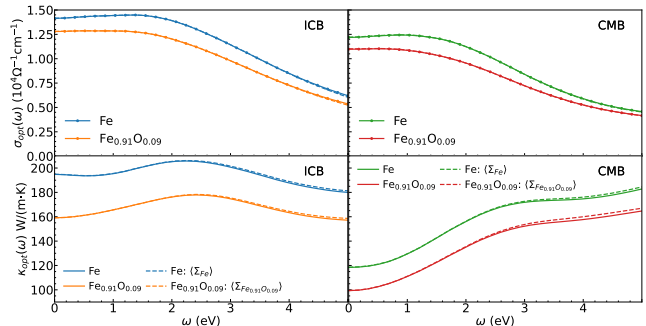


FIG. 2. Optical electrical (top) and thermal (bottom) conductivity for pure Fe and $\text{Fe}_{0.91}\text{O}_{0.09}$. The ICB and CMB cases are shown on the left and right, respectively. The dashed lines (that overlap closely with the filled ones) indicate a simplified calculation using fully (site, orbital, and spin) averaged self-energies.

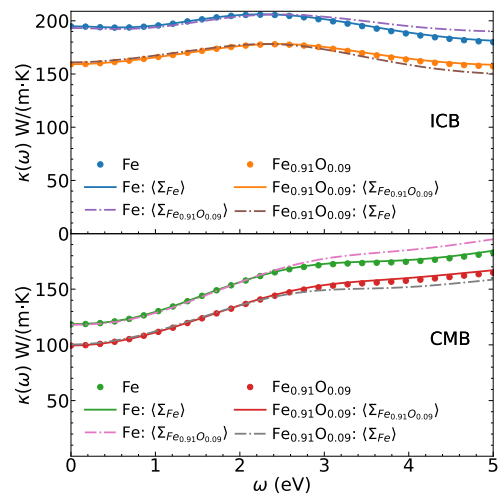


FIG. 3. Thermal conductivity for pure Fe and $\text{Fe}_{0.91}\text{O}_{0.09}$ for the ICB (top) and CMB (bottom) cases. We show the results obtained with orbitally and site-resolved self-energies (dots) as well as those calculated using the average self-energy (full line). The latter was first averaged over all sites and orbitals on the Matsubara grid and then analytically continued. The differences between the two are very small. With dash-dotted line, we show results calculated by exchanging the average self-energy between the Fe and $\text{Fe}_{0.91}\text{O}_{0.09}$.

To what extent is the suppression of conductivities in the oxygen-rich case due to the increase of EES documented in Fig. 1? It turns out that, as suggested in the earlier work [21] iron under Earth’s core conditions is in

a thermal-disorder dominated case where the changes of EES impact transport weakly. In Fig. 3 we demonstrate this by additional calculations where we compute the conductivity of the $\text{Fe}_{0.91}\text{O}_{0.09}$ case by using the scattering information from $\langle \Sigma \rangle$ corresponding to pure Fe calculation and vice versa for the other case. Quite strikingly, these “exchanged” calculations are at small frequencies almost indistinguishable from the “non-exchanged” ones. This tells that the oxygen affects the results through a structurally induced change in the band dispersions and that the changes in the EES play an insignificant role. This is further demonstrated in Appendix B where the scattering is artificially increased and only a weak effect on transport is seen.

Fig. 4 shows the calculated values of resistivity (top) and thermal conductivity (bottom) along with data from the literature. Thermal disorder dominates, and perfect crystalline lattices have much higher conductivities. The additional influence of compositional disorder is moderate, and the magnitude of the change is similar to that of including EES on top of the thermal disorder for a given composition.

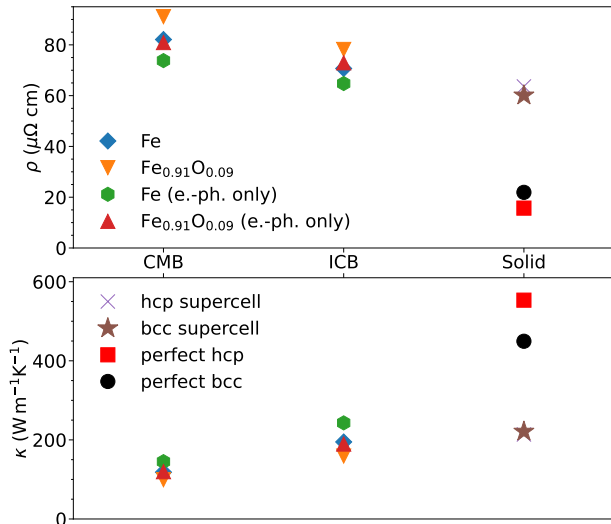


FIG. 4. Resistivity (top) and thermal conductivity (bottom) for Fe and $\text{Fe}_{0.91}\text{O}_{0.09}$ for the ICB and CMB cases calculated using DMFT (including both electron-electron and e-ph scattering) and DFT (e-ph. only). Previous calculations (extracted from Ref. [21]) for supercell and perfect lattice bcc/hcp are shown for the solid case.

Suppression of Lorenz ratio. Interestingly, EES suppresses the thermal conductivities more than the electrical ones. Figure 5 shows the evolution of the Lorenz number $L = \kappa/(\sigma T)$ with respect to the strength of EES, which is scaled by the factor α , as described in Appendix B. For pure Fe, the value of L due to electron-phonon scattering is almost identical to the standard value of $2.44 \cdot 10^{-8}$ ($\text{W}\Omega/\text{K}^2$), whereas it is considerably

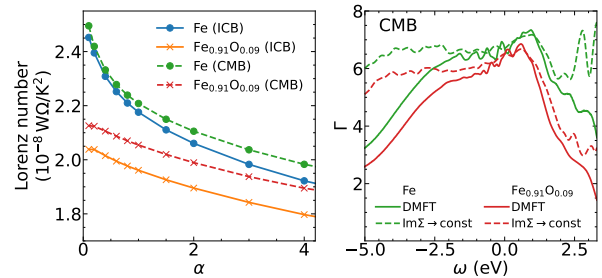


FIG. 5. (left) Lorenz number for Fe (bullets) and $\text{Fe}_{0.91}\text{O}_{0.09}$ (crosses) and for the ICB (full line) and CMB cases (dashed line). We use the parameter α to artificially change the magnitude of the EES $\Sigma \rightarrow \Sigma_\alpha = \text{Re}\Sigma + \alpha i \text{Im}\Sigma$. One sees that the Lorenz number is reduced by the presence of oxygen. (right) Transport distribution $\Gamma(\omega)$. Solid curves are the obtained form the full DMFT self energy, dashed lines from a constant scattering rate approximation.

reduced when EES is taken into account. This reduction occurs because inelastic EES affects κ more strongly than σ . Specifically, κ is determined by integrating $\Gamma(\omega)\omega^2(-df/d\omega)$, where $\Gamma(\omega)$ is the transport distribution function, f is the Fermi function, and ω is the frequency. On the other hand, σ is calculated by integrating $\Gamma(\omega)(-df/d\omega)$, which only involves the derivative of the Fermi function. The conductivity is mostly given by states around $\omega = 0$, while the dominant contribution to thermal conductivity occurs at finite energies $1.5T \lesssim |\omega| \lesssim 4T$.

The right panel of Figure 5 presents the transport distribution $\Gamma(\omega)$ for the CMB case, which are evaluated for the actual EES (full) and compared to a calculation where the energy dependence of scattering is suppressed and the self-energy $\text{Im}\Sigma \rightarrow \text{const}$ is taken (dashed), corresponding to a DFT transport distribution. It is evident that the increase of EES with energy suppresses Γ that becomes smaller at larger energies compared to the DFT transport distribution case. Additionally, a comparison between Fe and Fe-O is interesting, which is evident from the DFT transport distributions. The inclusion of oxygen leads to significant suppression of transport distribution at $\omega = 2.5\text{eV}$, caused by O-2p hybridization with the 4s iron states. This explains the smaller Lorenz number in the oxygen-rich case.

DISCUSSION

In summary, our study focused on the impact of oxygen on electronic transport in liquid iron corresponding to the outer Earth’s core conditions. Because oxygen diminishes the Fe 3d electronic occupation towards half-filling, it can be expected to strongly enhance electronic correlations. We indeed find that the EES is moderately increased. The numerical values of the conductivities and the Lorenz

Case	CMB $T=4400$ K $V=8.64 \text{ \AA}^3/\text{at}$		ICB $T=6350$ K $V=7.16 \text{ \AA}^3/\text{at}$	
	Fe	Fe _{0.91} O _{0.09}	Fe	Fe _{0.91} O _{0.09}
$-\text{Im}\langle\Sigma(\omega=0)\rangle$ (eV)	0.11	0.14	0.09	0.11
σ_{DFT} ($10^4\Omega^{-1}\text{cm}^{-1}$)	1.35	1.24	1.54	1.37
σ_{DMFT} ($10^4\Omega^{-1}\text{cm}^{-1}$)	1.22	1.10	1.41	1.28
$1 - \sigma_{\text{DMFT}}/\sigma_{\text{DFT}}$ (%)	10	11	9	7
κ_{DFT} ($\text{W m}^{-1}\text{K}^{-1}$)	145	120	243	190
κ_{DMFT} ($\text{W m}^{-1}\text{K}^{-1}$)	119	99	193	158
$1 - \kappa_{\text{DMFT}}/\kappa_{\text{DFT}}$ (%)	18	17	21	17
L_{DFT} ($10^{-8} \text{ W}\Omega\text{K}^{-2}$)	2.43	2.20	2.48	2.18
L_{DMFT} ($10^{-8} \text{ W}\Omega\text{K}^{-2}$)	2.22	2.05	2.16	1.95

TABLE I. Summary of results for CMB and ICB conditions, both for Fe and Fe_{0.91}O_{0.09}.

ratio are given in Table I. The oxygen substitution at $\sim 10\%$ level, which is a plausible content for the outer core, suppresses electrical (thermal) conductivities by about 10(17)% only. In both Fe and Fe-O including electronic correlations diminishes electrical conductivities by less than 10% and thermal conductivities by about 20%. This reduction is consistent with similar studies [21, 22], which suggests that it can be used as a rule of thumb when direct calculations are not feasible.

What are the geophysical implications of electronic correlations? The first observation is that their effect is moderate. The drastic reduction of conductivity, which was predicted on the basis of EES enhancement in ordered Fe-O structures [22], is not observed when thermal disorder effects are simultaneously included. But it is also clear from our study that neither can one neglect electronic correlations, since the reduction of conductivities due to EES is comparable to the reduction of electron-phonon scattering due to light elements. Importantly, some models that assume a higher heat flow from the core find a thermally only driven geodynamo for κ below a limiting value that is of order 100W/mK [44, 45]. EES whereas small compared to the thermal disorder, might in the end provide just the necessary additional scattering next to the compositional disorder to power the geodynamo sufficiently. At the very least, whenever one argues the compositional disorder is important, EES must not be neglected either. Another important finding is the universal suppression of Lorenz number: thermal conductivities are affected by EES more than electrical ones [19, 20]. This is seen to be also an effect of compositional disorder in the Fe-O case but EES enhances this further, by suppressing the contribution of states away from the Fermi energy. This is important both to properly interpret the high-pressure measurements that mostly probe σ and for the geodynamo, because of the distinct influence of the two quantities there.

In future studies, it would be interesting to investigate also alloying with sulfur and silicon [24]. Both elements

affect the transport properties strongly at the DFT level because unlike oxygen that alloys interstitially [24], they alloy substitutionally and therefore more strongly affect the bond disorder with perhaps different implications for electronic correlations. The silicon case was recently investigated [22], and the results for CMB seem compatible with what we find at comparable concentrations of oxygen, but sulfur that would act also in an oxidizing way could potentially have a bigger effect. Whereas the sulfur concentrations are believed to be negligible in the Earth [46], they are expected to be sizable in extraterrestrial planets [47]. Finally, both thermal disorder and compositional disorder are also important for Fe oxides that are relevant for the properties of the lower mantle, where, for example, FeO is predicted to be [48–51] in a state where electronic correlations are very strong and the influence of thermal and compositional disorder might lead to large effects there.

ACKNOWLEDGMENTS

GGB and JM are supported by Slovenian Research Agency (ARRS) under Grant no. P1-0044 and J1-2458. JM acknowledges discussions with A. Georges. DA and MP are supported by the U.K. Natural Environment Research Council (NERC) under Grant no. NE/T000228/1 and NE/R000425/1. Computations were performed on the supercomputer Vega at the Institute of Information Science (IZUM) in Maribor, Slovenia and in UK on the UK national service Archer2.

AUTHOR CONTRIBUTIONS

G.B.B. carried out the DFT + DMFT electronic structure and transport ‘calculations. D.A. and M.P. carried out the DFT molecular dynamics and transport calculations. G.G.B., J.M., L.V.P., M.A., and D.A. discussed the results and wrote the paper.

COMPETING INTERESTS

The authors declare no competing interests.

Appendix A: Matsubara self-energies

Figure 6 depicts the imaginary part of the self-energy as a function of Matsubara frequency at ICB (top) and CMB (bottom). The site, spin, and orbital average is performed and the corresponding self-energy is indicated by a full line, whereas the individual self-energies smoothly span the full range, indicated by shading. One sees the enhancement of EES for the oxygen-rich case in terms of larger magnitude (i.e. more negative values) of $\Sigma(i\omega)$.

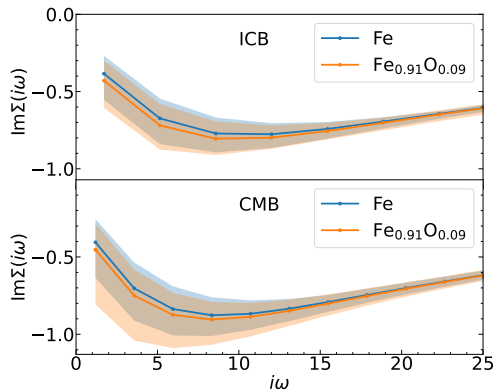


FIG. 6. Imaginary part of the Matsubara self-energy for the Fe (blue) and $\text{Fe}_{0.91}\text{O}_{0.09}$ (orange) configurations and ICB (top) and CMB cases (bottom). The lines represent the average over all sites, orbitals, and spins, while the shadow area shows the range of values. For both temperatures, the configuration with oxygen is below the pure iron one.

Appendix B: Effects of increased electron-electron scattering

In order to investigate how results depend on the strength of EES we performed trial conductivity calculation where we artificially set $\Sigma \rightarrow \Sigma_\alpha = \text{Re}\Sigma + \alpha i \text{Im}\Sigma$, thus increasing the scattering by a scale factor α . The calculated optical conductivities and thermal optical conductivities are shown in Fig. 7. One sees a weak dependence on α around $\alpha = 1$. As discussed in Ref. [21], the dependence of conductivities on the EES is weaker than what one would expect from Matthiessen's rule. The breakdown of Matthiessen's rule was also documented as a function of the substitutional disorder [11].

-
- [1] K. Ohta, Y. Kuwayama, K. Hirose, K. Shimizu, and Y. Ohishi, Experimental determination of the electrical resistivity of iron at earth's core conditions, *Nature* **534**, 95 (2016).
- [2] Z. Konôpková, R. S. McWilliams, N. Gómez-Pérez, and A. F. Goncharov, Direct measurement of thermal conductivity in solid iron at planetary core conditions, *Nature (London)* **534**, 99 (2016).
- [3] S. S. Lobanov and Z. M. Geballe, Non-isotropic contraction and expansion of samples in diamond anvil cells: Implications for thermal conductivity at the core-mantle boundary, *Geophysical Research Letters* **49**, 10.1029/2022gl100379 (2022).
- [4] D. Alfè and M. J. Gillan, First-principles simulations of liquid fe-s under earth's core conditions, *Phys. Rev. B* **58**, 8248 (1998).
- [5] M. Pozzo, C. Davies, D. Gubbins, and D. Alfè, Thermal and electrical conductivity of iron at earth's core conditions, *Nature* **485**, 355 (2012).
- [6] N. de Koker, G. Steinle-Neumann, and V. Vlček, Electrical resistivity and thermal conductivity of liquid fe alloys at high p and t, and heat flux in earth's core, *Proc. Natl. Acad. Sci. U. S. A.* **109**, 4070 (2012).
- [7] F. D. Stacey and O. L. Anderson, Electrical and thermal conductivities of fe-ni-si alloy under core conditions, *Physics of the Earth and Planetary Interiors* **124**, 153 (2001).
- [8] F. Stacey and D. Loper, A revised estimate of the conductivity of iron alloy at high pressure and implications for the core energy balance, *Physics of the Earth and Planetary Interiors* **161**, 13 (2007).
- [9] O. Gunnarsson, M. Calandra, and J. E. Han, Colloquium: Saturation of electrical resistivity, *Rev. Mod. Phys.* **75**, 1085 (2003).
- [10] H. Gomi, K. Ohta, K. Hirose, S. Labrosse, R. Caracas, M. J. Verstraete, and J. W. Hernlund, The high conductivity of iron and thermal evolution of the earth's core, *Physics of the Earth and Planetary Interiors* **224**, 88 (2013).
- [11] H. Gomi, K. Hirose, H. Akai, and Y. Fei, Electrical resistivity of substitutionally disordered hcp fe-si and fe-ni alloys: Chemically-induced resistivity saturation in the earth's core, *Earth and Planetary Science Letters* **451**, 51 (2016).
- [12] J. A. Tarduno, R. D. Cottrell, M. K. Watkeys, A. Hofmann, P. V. Doubrovine, E. E. Mamajek, D. Liu, D. G. Sibeck, L. P. Neukirch, and Y. Usui, Geodynamo, solar wind, and magnetopause 3.4 to 3.45 billion years ago, *Science* **327**, 1238 (2010).
- [13] J. A. Tarduno, R. D. Cottrell, W. J. Davis, F. Nimmo, and R. K. Bono, A hadean to paleoarchean geodynamo recorded by single zircon crystals, *Science* **349**, 521 (2015).
- [14] P. Olson, The new core paradox, *Science* **342**, 431 (2013).
- [15] L. Pourovskii, T. Miyake, S. Simak, A. V. Ruban, L. Dubrovinsky, and I. Abrikosov, Electronic properties and magnetism of iron at the earth's inner core conditions, *Physical Review B* **87**, 115130 (2013).
- [16] L. V. Pourovskii, Electronic correlations in dense iron: from moderate pressure to earth's core conditions, *Journal of Physics: Condensed Matter* **31**, 373001 (2019).
- [17] X. Deng, J. Mravlje, R. Žitko, M. Ferrero, G. Kotliar, and A. Georges, How bad metals turn good: Spectroscopic signatures of resilient quasiparticles, *Phys. Rev. Lett.* **110**, 086401 (2013).
- [18] P. Zhang, R. Cohen, and K. Haule, Effects of electron correlations on transport properties of iron at earth's core conditions, *Nature (London)* **517**, 605 (2015).
- [19] L. V. Pourovskii, J. Mravlje, A. Georges, S. I. Simak, and I. A. Abrikosov, Electron-electron scattering and thermal conductivity of ϵ -iron at earth's core conditions, *New Journal of Physics* **19**, 073022 (2017).

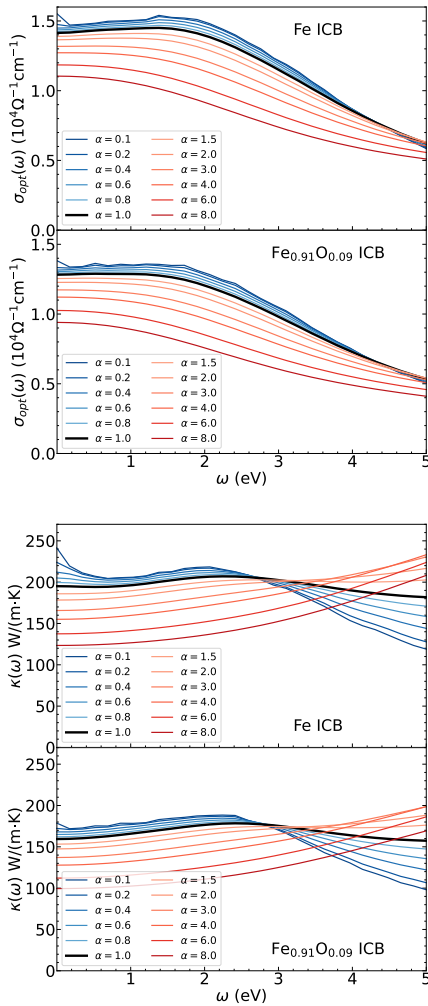


FIG. 7. The optical conductivity and thermal optical conductivity of Fe and $\text{Fe}_{0.91}\text{O}_{0.09}$ configuration with a scale factor α applied to the imaginary part of calculated average self-energy.

- [20] J. Xu, P. Zhang, K. Haule, J. Minar, S. Wimmer, H. Ebert, and R. E. Cohen, Thermal conductivity and electrical resistivity of solid iron at earth's core conditions from first principles, *Phys. Rev. Lett.* **121**, 096601 (2018).
- [21] L. V. Pourovskii, J. Mravlje, M. Pozzo, and D. Alfè, Electronic correlations and transport in iron at earth's core conditions, *Nature Communications* **11**, 4105 (2020).
- [22] Y. Zhang, K. Luo, M. Hou, P. Driscoll, N. P. Salke, J. Minár, V. B. Prakapenka, E. Greenberg, R. J. Hemley, R. E. Cohen, and J.-F. Lin, Thermal conductivity of fe-si alloys and thermal stratification in earth's core, *Proceedings of the National Academy of Sciences* **119**, e2119001119 (2022), <https://www.pnas.org/doi/pdf/10.1073/pnas.2119001119>.
- [23] J. Badro, J. P. Brodholt, H. Piet, J. Siebert, and F. J. Ryerson, Core formation and core composition from coupled geochemical and geophysical constraints, *Proceedings of the National Academy of Sciences* **112**, 12310 (2015).
- [24] F. Wagle, G. Steinle-Neumann, and N. de Koker, Resistivity saturation in liquid iron–light-element alloys at conditions of planetary cores from first principles computations, *Comptes Rendus Geoscience* **351**, 154 (2019).
- [25] W.-J. Li, Z. Li, X.-T. He, C. Wang, and P. Zhang, Constraints on the thermal evolution of earth's core from ab initio calculated transport properties of FeNi liquids, *Earth and Planetary Science Letters* **562**, 116852 (2021).
- [26] A. Georges, L. de' Medici, and J. Mravlje, Strong correlations from hund's coupling, *Annual Review of Condensed Matter Physics* **4**, 137 (2013).
- [27] B. G. Jang, Y. He, J. H. Shim, H.-k. Mao, and D. Y. Kim, Oxygen-driven enhancement of electron correlation in hexagonal iron at earth's inner core conditions (2021), arXiv:2111.11033.
- [28] A. Georges, G. Kotliar, W. Krauth, and M. J. Rozenberg, Dynamical mean-field theory of strongly correlated fermion systems and the limit of infinite dimensions, *Reviews of Modern Physics* **68**, 13 (1996).
- [29] A. Hausoel, M. Karolak, E. Şaşıoğlu, A. Lichtenstein, K. Held, A. Katanin, A. Toschi, and G. Sangiovanni, Local magnetic moments in iron and nickel at ambient and earth's core conditions, *Nature Communications* **8**, 10.1038/ncomms16062 (2017).
- [30] G. Kresse and J. Furthmüller, Efficient iterative schemes for ab initio total-energy calculations using a plane-wave basis set, *Phys. Rev. B* **54**, 11169 (1996).
- [31] G. Kresse and D. Joubert, From ultrasoft pseudopotentials to the projector augmented-wave method, *Phys. Rev. B* **59**, 1758 (1999).
- [32] P. E. Blöchl, Projector augmented-wave method, *Phys. Rev. B* **50**, 17953 (1994).
- [33] S. Nosé, A molecular dynamics method for simulations in the canonical ensemble, *Molecular Physics* **52**, 255 (1984).
- [34] M. P. Desjarlais, J. D. Kress, and L. A. Collins, Electrical conductivity for warm, dense aluminum plasmas and liquids, *Phys. Rev. E* **66**, 025401 (2002).
- [35] P. Blaha, K. Schwarz, G. Madsen, D. Kvasnicka, and J. Luitz, WIEN2k, An augmented Plane Wave + Local Orbitals Program for Calculating Crystal Properties (Techn. Universitat Wien, Austria, 2001).
- [36] P. Blaha, K. Schwarz, F. Tran, R. Laskowski, G. K. H. Madsen, and L. D. Marks, Wien2k: An apw+lo program for calculating the properties of solids, *The Journal of Chemical Physics* **152**, 074101 (2020), <https://doi.org/10.1063/1.5143061>.
- [37] O. Parcollet, M. Ferrero, T. Ayril, H. Hafermann, I. Krivenko, L. Messio, and P. Seth, Triqs: A toolbox for research on interacting quantum systems, *Computer Physics Communications* **196**, 398 (2015).
- [38] M. Aichhorn, L. Pourovskii, V. Vildosola, M. Ferrero, O. Parcollet, T. Miyake, A. o. Georges, and S. Biermann, Dynamical mean-field theory within an augmented plane-wave framework: Assessing electronic correlations in the iron pnictide lafeaso, *Phys. Rev. B* **80**, 085101 (2009).
- [39] M. Aichhorn, L. Pourovskii, and A. Georges, Importance of electronic correlations for structural and magnetic properties of the iron pnictide superconductor lafeaso, *Phys. Rev. B* **84**, 054529 (2011).
- [40] M. Aichhorn, L. Pourovskii, P. Seth, V. Vildosola, M. Zingl, O. E. Peil, X. Deng, J. Mravlje, G. J. Kraberger, C. Martins, M. Ferrero, and O. Parcollet,

- Triqs/dfttools: A {TRIQS} application for ab initio calculations of correlated materials, *Computer Physics Communications* **204**, 200 (2016).
- [41] P. Werner, A. Comanac, L. de' Medici, M. Troyer, and A. J. Millis, Continuous-time solver for quantum impurity models, *Phys. Rev. Lett.* **97**, 076405 (2006).
- [42] P. Werner and A. J. Millis, Hybridization expansion impurity solver: General formulation and application to kondo lattice and two-orbital models, *Phys. Rev. B* **74**, 155107 (2006).
- [43] G. Kotliar, S. Y. Savrasov, K. Haule, V. S. Oudovenko, O. Parcollet, and C. Marianetti, Electronic structure calculations with dynamical mean-field theory, *Reviews of Modern Physics* **78**, 865 (2006).
- [44] P. Driscoll and D. Bercovici, On the thermal and magnetic histories of earth and venus: Influences of melting, radioactivity, and conductivity, *Physics of the Earth and Planetary Interiors* **236**, 36 (2014).
- [45] M. Landeau, A. Fournier, H.-C. Nataf, D. Cébron, and N. Schaeffer, Sustaining earth's magnetic dynamo, *Nature Reviews Earth & Environment* **3**, 255 (2022).
- [46] G. Dreibus and H. Palme, Cosmochemical constraints on the sulfur content in the earth's core, *Geochimica et Cosmochimica Acta* **60**, 1125 (1996).
- [47] O. Namur, B. Charlier, F. Holtz, C. Cartier, and C. McCammon, Sulfur solubility in reduced mafic silicate melts: Implications for the speciation and distribution of sulfur on mercury, *Earth and Planetary Science Letters* **448**, 102 (2016).
- [48] K. Ohta, R. E. Cohen, K. Hirose, K. Haule, K. Shimizu, and Y. Ohishi, Experimental and theoretical evidence for pressure-induced metallization in feo with rocksalt-type structure, *Phys. Rev. Lett.* **108**, 026403 (2012).
- [49] I. Leonov, A. V. Ponomareva, R. Nazarov, and I. A. Abrikosov, Pressure-induced spin-state transition of iron in magnesio-wüstite (fe,mg)o, *Phys. Rev. B* **96**, 075136 (2017).
- [50] I. Leonov, A. O. Shorikov, V. I. Anisimov, and I. A. Abrikosov, Emergence of quantum critical charge and spin-state fluctuations near the pressure-induced mott transition in mno, feo, coo, and nio, *Phys. Rev. B* **101**, 245144 (2020).
- [51] W. D. Ho, P. Zhang, K. Haule, J. Jackson, V. Dobrosavljevic, and V. Dobrosavljevic, Quantum critical phase of FeO spans conditions of Earth's lower mantle, arXiv:2301.047771.